ADVANCED FUNCTIONAL MATERIALS
www.afm-journal.de

FULL PAPER

Flexible Cellulose Paper-based Asymmetrical Thin Film Supercapacitors with High-Performance for Electrochemical Energy Storage

*Jin-Xian Feng, Sheng-Hua Ye, An-Liang Wang, Xue-Feng Lu, Ye-Xiang Tong, and Gao-Ren Li**

Cellulose paper (CP)-based asymmetrical thin film supercapacitors (ATFSCs) have been considered to be a novel platform for inexpensive and portable devices as the CP is low-cost, lightweight, and can be rolled or folded into 3D configurations. However, the low energy density and poor cycle stability are serious bottlenecks for the development of CP-based ATFSCs. Here, sandwich-structured graphite/Ni/Co_2NiO_4-CP is developed as positive electrode and the graphite/Ni/AC-CP as negative electrode for flexible and high-performance ATFSCs. The fabricated graphite/Ni/Co_2NiO_4-CP positive electrode shows a superior areal capacitance (734 mF/cm^2 at 5 mV/s) and excellent cycling performance with ≈97.6% C_{sp} retention after 15 000 cycles. The fabricated graphite/Ni/AC-CP negative electrode also exhibits large areal capacitance (180 mF/cm^2 at 5 mV/s) and excellent cycling performance with ≈98% C_{sp} retention after 15 000 cycles. The assembled ATFSCs based on the sandwich-structured graphite/Ni/Co_2NiO_4-CP as positive electrode and graphite/Ni/AC-CP as negative electrode exhibit large volumetric C_{sp} (7.6 F/cm^3 at 5 mV/s), high volumetric energy density (2.48 mWh/cm^3, 80 Wh/kg), high volumetric power density (0.79 W/cm^3, 25.6 kW/kg) and excellent cycle stability (less 4% C_{sp} loss after 20 000 cycles). This study shows an important breakthrough in the design and fabrication of high-performance and flexible CP-based electrodes and ATFSCs.

1. Introduction

The development of miniaturized/portable electronic devices, such as flexible/wearable electronics and active artificial skins, eagerly requires a high performance, compact, light and integrable energy storage/supply module to ensure their functionality.[1,2] The conventional energy storage/supply devices, such as batteries and supercapacitors (SCs), are very difficult to provide the power needed for the miniaturized/portable electronic devices because they are too heavy or bulky.[3,4] Recently, the flexible thin film energy storage/supply devices as a new emerging branch are attracting more and more interest because they are propitious to make the whole entire device to be light, thin and flexible and are much favorable for the development of miniaturized/portable electronic devices.[5,6]

SCs as promising energy-storage devices have attracted tremendous interest because of their high power density and capability to quickly charge and discharge, which are favorable characteristics of devices that are utilized in portable electronics, hybrid vehicles, and backup energy systems.[7–15] Recently, the cellulose paper (CP)-based thin film SCs have been considered to be a novel platform for inexpensive and portable devices as the CP is widely available, flexible, low-cost, lightweight, biodegradable, and can be rolled or folded into 3D configurations.[16–18] However, the low energy density and poor cycle stability are serious bottlenecks for the applications of CP-based thin film SCs. Comparing with conventional SCs, the asymmetric SCs can operate in much wider potential windows, which will lead to a substantial increase in the energy density.[19,20] In addition, the incorporation of advanced functional materials and nanotechnologies will allow scientists to enhance the energy density and cycle stability of CP-based thin film SCs.[21–23] However, the high surface roughness and insulation of CP are major concerns for material interconnections and functional device fabrication. This makes integration of functional electronic counterparts on CP difficult. To overcome the above limitations and improve the electrochemical performance, recently many studies have focused on developing functional CP electrodes. For example, Cui et al. demonstrated the concept of fabricating conductive CP electrodes by directly drawing graphite on CP with a pencil,[21] Zhou et al. developed functional CP electrodes through polypyrrole (PPy) coating on CP by a simple and low-cost “soak and polymerization” method,[22] and Wang et al. fabricated highly flexible all-solid-state SCs based on the PANI/Au/paper.[23] Despite great progress, metal oxide coating and

J.-X. Feng, S.-H. Ye, A.-L. Wang, X.-F. Lu,
Prof. Y.-X. Tong, Prof. G.-R. Li
MOE Laboratory of Bioinorganic
and Synthetic Chemistry
KLGHEI of Environment and Energy Chemistry
School of Chemistry and Chemical Engineering
Sun Yat-sen University
Guangzhou 510275, China
E-mail: ligaoren@mail.sysu.edu.cn

DOI: 10.1002/adfm.201401876

multi-layered coating on CP and the fabrication of CP-based asymmetrical thin film SCs with high-performance still face a huge challenge. It is highly desirable to develop the CP-based asymmetrical thin film SCs with superior cycle stability and high energy density without sacrificing their power density.

In this study, we develop novel sandwich-structured graphite/Ni/Co_2NiO_4-CP as positive electrode and graphite/Ni/active carbon (AC)-CP as negative electrode for flexible and high-efficient asymmetrical thin film supercapacitors (ATFSCs). We firstly demonstrated a simple drawing-electrodeposition-anodic oxide combined method to fabricate the multi-layered graphite/Ni/Co_2NiO_4-CP electrodes and a drawing-electrodeposition-drawing combined method to fabricate the multi-layered graphite/Ni/AC-CP electrodes. The idea here was inspired by the fact that graphite layer is easy to be coated on CP by simple drawing method and then Ni and Co_2NiO_4 layers can be easily electrodeposited on it. It has been reported that nickel-cobalt binary metal oxides have greater electron conductivity and electrochemical activity than nickel and cobalt oxides. The nickel-cobalt binary metal oxides are generally regarded as a kind of mixed valence oxide that adopts a pure spinel structure and is expected to offer richer redox chemistry than the two single component oxides due to the combined contributions from both nickel and cobalt ions. Co_2NiO_4 has been considered to be one of the most attractive electrode materials for SCs because of its low cost, high abundance, high theoretical specific capacitance (C_{sp}), and environmental friendliness. AC is a promising negative electrode because of their large surface area, excellent electrical conductivity, and outstanding electrochemical stability. Here the flexible ATFSCs assembled by sandwich-structured graphite/Ni/Co_2NiO_4-CP as positive electrodes and graphite/Ni/AC-CP as negative electrodes exhibit large volumetric C_{sp} of 7.6 F/cm^3 (equal to 247 F/g at 5 mV/s), superior long-term cycle stability (less 4% loss of the maximum C_{sp} after 20 000 cycles), high energy density (2.48 mWh/cm^3, 80 Wh/kg), and high power density (0.79 W/cm^3, 25.6 kW/kg). These findings indicate that the sandwich-structured graphite/Ni/Co_2NiO_4-CP and graphite/ Ni/AC-CP electrodes are promising for the flexible ATFSCs.

2. Results and Discussion

The fabrication procedure of graphite/Ni/Co_2NiO_4-CP electrode is shown in **Figure 1**a: i) The homogeneous graphite layer is firstly coated on CP to form the graphite-CP by drawing method; ii) Then the homogeneous Ni layer is coated on the surface of graphite-CP to form graphite/Ni-CP; iii) Co_2NiO_4 nanosheets are further coated on the surface of graphite/Ni-CP by electrodeposition and anodic anodization and accordingly the sandwich-structured graphite/Ni/Co_2NiO_4-CP electrode is fabricated (details in Experimental Section and Supporting Information (SI)). Optical images of CP and graphite-CP are shown in Figure 1b and 1c, respectively, and they show the graphite layer on CP is very uniform. The mass loading of graphite is 0.15 mg/cm^2. The electrical resistance of graphite-CP (2.0 cm × 0.5 cm) is ≈170 Ω/sq. So the resistance of CP (>20 MΩ/sq) is greatly reduced by coating graphite layer. Optical image of graphite/Ni-CP is shown in Figure 1d, and it indicates Ni layer is also uniform. After coating Ni layer, the resistance of sample is further obviously reduced and it is only ≈1.0 Ω/sq. Optical image of graphite/Ni/Co_2NiO_4-CP is shown in Figure 1e, and it demonstrates that the Co_2NiO_4 layer is uniformly coated on the surface of graphite/Ni-CP. The electronic and ionic conductivities of the graphite/Ni/Co_2NiO_4-CP electrode are studied by electrochemical impedance spectroscopy (EIS). Nyquist plot of the graphite/Ni/Co_2NiO_4-CP electrode between 0.01 and 10 000 Hz is shown in Figure S1, which shows the graphite/Ni/Co_2NiO_4-CP electrode has high electron and ionic conductibility. The high conductibility in electrode will favor rate capability for high power performance and fast charge–discharge, and the utilization rate of electrode material will also be largely enhanced because of the slight polarization.

Figure 1f,g shows SEM images of surface morphologies of CP and graphite-CP, respectively. We can clearly see that the surface of CP is rough and porous. After coating graphite layer, the surface becomes uniform as shown in Figure 1g. SEM image of the cross section of graphite-CP is shown in Figure 1h, which shows the thicknesses of graphite layer is about 2.0 µm. The surface of Ni layer is also uniform as shown in Figure 1i. SEM image of the cross section of graphite/Ni-CP is shown in Figure 1j, which shows the thicknesses of Ni layer is about 1.0 µm. Figure 1k shows the Co_2NiO_4 layer grown on the surface of graphite/Ni-CP is porous structure that is consisted of nanosheets, which would relax the transport of ions, enable fast electrochemical reactions and provide short diffusion paths for ions. The porous structures would also obviously enhance the utilization rate of Co_2NiO_4. SEM images of the cross sections of the graphite/Ni/Co_2NiO_4-CP and the magnified Ni/Co_2NiO_4 layers are shown in Figure 1l and 1m, respectively, which show the thickness of Co_2NiO_4 layer is ≈1.5 µm. Figures 1n–p show TEM, HRTEM and SAED images of Co_2NiO_4 nanosheets in the graphite/Ni/Co_2NiO_4-CP. The lattice fringe spacing of Co_2NiO_4 nanosheets was measured to be 0.25 nm as shown in Figure 1o, which is consistent with the *d*-spacing of (400) plane of Co_2NiO_4. SAED analysis confirms that the Co_2NiO_4 nanosheeet is single-crystal as shown in Figure 1p. The sandwich-structured graphite/Ni/Co_2NiO_4 layers grown on CP are rather firmly and the graphite/Ni/Co_2NiO_4-CP electrode shows good flexibility as shown in Figure S2.

Raman spectra of graphite layer in the graphite-CP is shown in Figure S3, which shows two peaks at 1353 and 1580 cm^{-1} and proves the existence of graphite layer. EDS spectrum of Ni layer in the graphite/Ni-CP and XRD patterns of CP, graphite-CP and graphite/Ni-CP shown in Figure S4 prove the existence of Ni layer. XRD pattern of the graphite/Ni/Co_2NiO_4-CP is shown in **Figure 2**a(iv). The peak located at 44.8° can be indexed to the (400) plane of Co_2NiO_4 and the small peaks at 52.3° and 77.2° can be indexed to (422) and (533) planes of Co_2NiO_4, respectively (JCPDS #2–1074). To better understand the chemical composition of Co_2NiO_4 layers, X-ray photoelectron spectroscopy (XPS) was conducted and the results are shown in Figure 2b–d. Figure 2b shows Co 2p spectrum of Co_2NiO_4 nanosheeets. The peak at the binding energy of 780.1 eV can be ascribed to Co^{3+}. The peak at the binding energy of 782.2 eV and the satellite structures

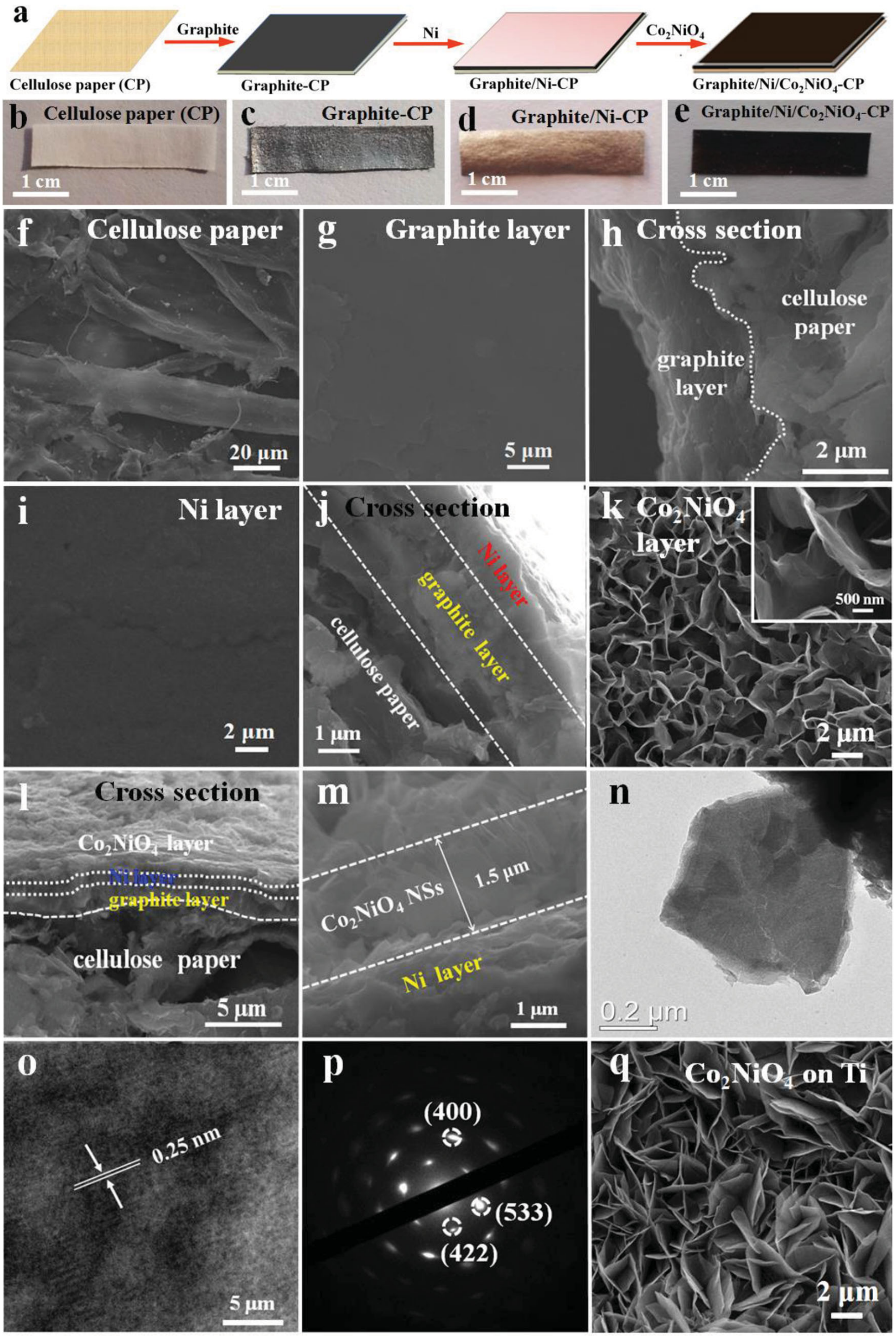

Figure 1. a) Schematic illustration for the fabrication of graphite/Ni/Co_2NiO_4-CP electrode; Optical images of b) CP, c) graphite-CP, d) graphite/Ni-CP, and e) graphite/Ni/Co_2NiO_4-CP; SEM images of f) CP, g) graphite layer, h) cross section of graphite-CP, i) Ni layer, j) cross section of graphite/Ni-CP, k) Co_2NiO_4 layer, l) cross section of graphite/Ni/Co_2NiO_4-CP, and m) the magnified cross section of Ni/Co_2NiO_4 layer; n) TEM, o) HRTEM, and p) SAED images of a typical Co_2NiO_4 nanosheet; q) SEM image of Co_2NiO_4 nanosheets grown on Ti plate.

can be ascribed to Co^{2+}, indicating the co-existence of Co^{2+} and Co^{3+} ions in Co_2NiO_4 nanosheeets.[24–26] Ni 2p spectrum of the Co_2NiO_4 nanosheeets is shown in Figure 2c. The Ni $2p_{3/2}$ peak at 855.9 and Ni $2p_{3/2}$ peak at 857.4 eV inidcate the coexistence of Ni^{2+} and Ni^{3+}.[27–29] XPS spectrum of O1s in Figure 2d shows the peak O_I at 529.2 eV corresponds to nickel-oxygen bonds while the peak O_{II} at 531.2 eV is ascribed to cobalt-oxygen bonds.[24,25,30] XPS analysis also show that the atom ratio of Co, Ni and O is 22.9 at%, 11.3 at% and 46.3 at%, which is enclosed to 2:1:4. Based the above XPS results,

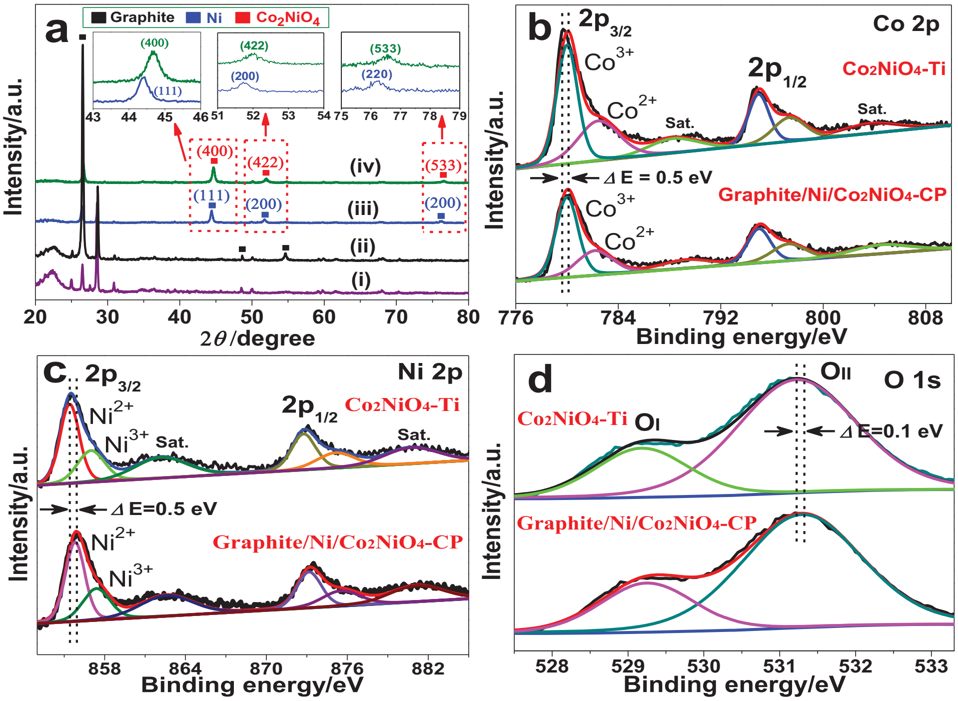

Figure 2. a) XRD patterns of i) CP, ii) graphite-CP, iii) graphite/Ni-CP, and iv) graphite/Ni/Co_2NiO_4-CP; XPS spectra of b) Co2p, c) Ni 2p, and d) O1s of Co_2NiO_4 nanosheets in the graphite/Ni/Co_2NiO_4-CP and Co_2NiO_4-Ti.

the structure of Co_2NiO_4 can be determined as $Co(III)_xNi(III)_y[Co(II)_{2-x}Ni(II)_{1-y}]O_4$.

To study the effect of Ni layer on the electronic state of Co_2NiO_4 layer in graphite/Ni/Co_2NiO_4-CP electrode, the Co_2NiO_4 nanosheets on Ti sheet (Co_2NiO_4-Ti) were also fabricated as shown in Figure 1q (the resistance of Ti sheet is 0.03 Ω/sq). XPS spectra of Co_2NiO_4-Ti in Co2p, Ni2p, and O1s regions were also measured as shown in Figure 2b–d, respectively. As shown in Figure 2b, Co $2p_{1/2}$ and $2p_{3/2}$ peaks of graphite/Ni/Co_2NiO_4-CP both shift to higher binding energies (780.1 and 795.1 eV) relative to Co $2p_{1/2}$ and $2p_{3/2}$ peaks of Co_2NiO_4-Ti (779.6 and 794.6 eV). As shown in Figure 2c, the Ni $2p_{1/2}$ and $2p_{3/2}$ peaks of Co_2NiO_4 in the graphite/Ni/Co_2NiO_4-CP both shift to higher binding energies (855.9 and 873.2 eV) relative to Ni $2p_{1/2}$ and $2p_{3/2}$ peaks of Co_2NiO_4-Ti (855.4 and 872.7 eV). In addition, the O 1s peaks of the graphite/Ni/Co_2NiO_4-CP shift 0.1 eV compared with those of Co_2NiO_4-Ti as shown in Figure 2d. So the shifts of Co 2p, Ni 2p, and O1s peaks in binding energies confirm strong electron interactions involving Co_2NiO_4 layer and Ni layer in the graphite/Ni/Co_2NiO_4-CP.[25] These interactions will change electronic states of Co, Ni and O atoms and accordingly will improve the electrochemical properties of graphite/Ni/Co_2NiO_4-CP.

Electrochemical property of the graphite/Ni/Co_2NiO_4-CP electrodes was studied in 1.0 M KOH aqueous electrolyte by a three-electrode configuration with a Pt counter-electrode and a saturated calomel electrode (SCE) as reference electrode. Compared with graphite-CP and graphite/Ni-CP electrodes, the graphite/Ni/ Co_2NiO_4-CP electrode shows much larger current density as shown in **Figure** 3a, indicating that Co_2NiO_4 is the main contributor for electrochemical capacitance. The graphite and Ni layers contribute much less capacitance compared with Co_2NiO_4. Here the graphite layer is crucial for the coating of Ni and Co_2NiO_4 on CP and can enhance the conductivity of CP. The Ni layer further enhances the conductivity of electrode and can improve the electrochemical performance of Co_2NiO_4. To study the effect of Ni on the electrochemical property of Co_2NiO_4, Figure 3b shows cyclic voltammograms (CVs) of the graphite/Ni/Co_2NiO_4-CP, graphite/Co_2NiO_4-CP, and Co_2NiO_4-Ti electrodes with the same loading of Co_2NiO_4 (0.35 mg/cm^2) at a scan rate of 100 mV/s. As is expected, the graphite/Ni/Co_2NiO_4-CP electrode shows a much larger current density than those of graphite/Co_2NiO_4-CP and Co_2NiO_4-Ti electrodes, demonstrating an obvious enhancement of electrochemical capacitance because of the effect of Ni layer on the electronic state of Co_2NiO_4 layer. Without Ni layer, the graphite/Co_2NiO_4-CP electrode almost has no capacitance because its resistance is quite high. In addition, CVs of the graphite/Ni/Co_2NiO_4-CP electrode measured at different scan rates exhibit rectangular-like shapes and keep similar with increasing scan rate from 5 to 100 mV/s as shown in Figure 3c, indicating good capacitive performance and high-rate capability. The areal capacitance and rate capability of the graphite/Ni/Co_2NiO_4-CP, graphite/Co_2NiO_4-CP, and Co_2NiO_4-Ti electrodes are compared as shown in Figure 3d. The graphite/Ni/Co_2NiO_4-CP electrode shows much larger areal capacitances than the graphite/Co_2NiO_4-CP and Co_2NiO_4-Ti electrodes at different scan rates. The largest areal capacitance measured for the graphite/Ni/Co_2NiO_4-CP electrode is 734 mF/cm^2 (≈2097 F/g for the Co_2NiO_4) at 5 mV/s. Galvanostatic charge–discharge curves of the graphite/Ni/Co_2NiO_4-CP electrodes at different current densities are shown in Figure 3e, and they

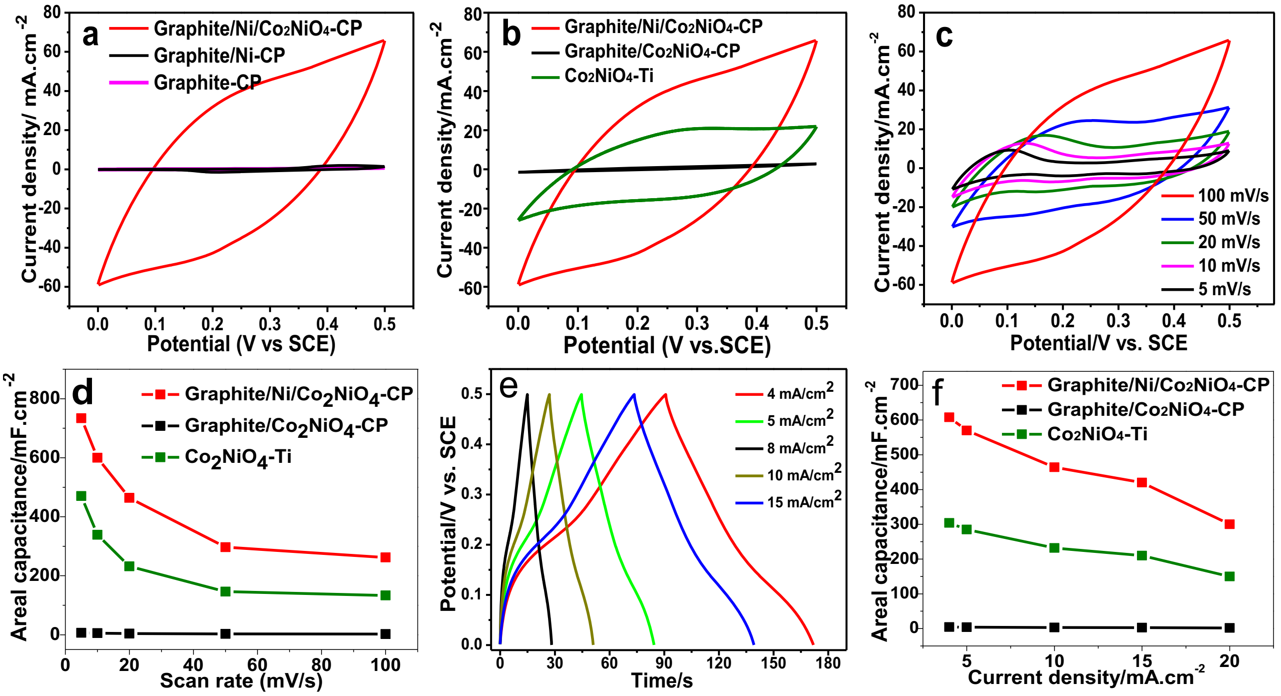

Figure 3. a) CVs of graphite-CP, graphite/Ni-CP, and graphite/Ni/Co_2NiO_4-CP electrodes at 100 mV/s; b) CVs of graphite/Ni/Co_2NiO_4-CP, graphite/Co_2NiO_4-CP, and Co_2NiO_4-Ti electrodes at a scan rate of 100 mV/s; c) CVs of graphite/Ni/Co_2NiO_4-CP electrode at scan rates of 5–100 mV/s; d) Areal capacitance and capacitance retention of graphite/Ni/Co_2NiO_4-CP, graphite/Co_2NiO_4-CP, and Co_2NiO_4-Ti electrodes calculated from CV curves as a function of scan rate; e) Galvanostatic charge–discharge curves of graphite/Ni/Co_2NiO_4-CP electrode at different current densities of 4–15 mA/cm^2; f) Areal capacitance and capacitance retention of graphite/Ni/Co_2NiO_4-CP, graphite/Co_2NiO_4-CP, and Co_2NiO_4-Ti electrodes calculated from the galvanostatic charge–discharge curves as a function of current density.

all are well symmetrical. This confirms the superior reversible redox reactions and good supercapacitive characteristic of the graphite/Ni/Co_2NiO_4-CP electrodes. The summary plot of C_{sp} vs current density is shown in Figure 3f, which also demonstrates the graphite/Ni/Co_2NiO_4-CP electrode exhibits significantly enhanced supercapacitive performance comparing with the graphite/Co_2NiO_4-CP and Co_2NiO_4-Ti electrodes. At current density of 4 mA/cm^2, graphite/Ni/Co_2NiO_4-CP electrode shows areal capacitance of 608 mF/cm^2 (≈1737 F/g for the Co_2NiO_4), which is much larger than the values obtained for graphite/Co_2NiO_4-CP and Co_2NiO_4-Ti electrodes as shown in Figure 3f and is also much larger than those prviously reported for other CP-based electrodes, such as graphite-CP electrode (<5 mF/cm^2 at 4.0 mA/g)[21] and PANI-Au-CP electrode (~480 mF/cm^2 at 4.0 mA/cm^2).[23] In addition, the graphite/Ni/Co_2NiO_4-CP electrode shows excellent cycle life as shown in Figure S5, which shows only 2.4% decrease after 15 000 cycles. This cycling performance is much better than those of the reported CP-electrodes.[21,22,31,32] The above results assuredly show that the introduction of graphite, Ni and Co_2NiO_4 layers on CP can substantially enhance the conductivity and electrochemical performance of CP electrode.

The graphite/Ni/AC-CP as negative electrode was also fabricated via similar procedures of the graphite/ Ni/Co_2NiO_4-CP electrodes as shown in Figure S6 (The loading mass of AC is ≈1.20 g/cm^2). SEM image in Figure S7 shows AC layer is uniform. Nyquist plot in Figure S8 shows a low equivalent series resistance and a vertical line in the low-frequency region, indicating that the graphite/Ni/AC-CP electrode has a high electronic and ionic conductivity. After various bending states, the AC layer still remains unchanged, indicating good adhesion and high flexible (Figure S9). A series of various CVs of graphite/Ni/AC-CP electrode with different potential windows were measured as shown in **Figure** 4a. Here we find the operating potentials of the graphite/Ni/AC-CP electrode can be chosen from −1.5 to 0 V. The linear sweep voltammogram in Figure S10 shows the potential of hydrogen evolution on the graphite/Ni/AC-CP electrode is approximately −1.67 V versus SCE, demonstrating the operating potential of −1.5 to 0 V is advisable. Figure 4b shows the graphite/Ni/AC-CP electrode has much larger capacitance than graphite-CP and graphite/Ni-CP electrodes, indicating AC layer contributes much more capacitance than graphite and Ni layers. CVs of graphite/Ni/Co_2NiO_4-CP electrode at different scan rates exhibit rectangular-like shapes and keep similar with increasing scan rate from 5 to 100 mV/s as shown in Figure 4c, indicating good capacitive performance. At scan rate of 5 mV/s, C_{sp} of graphite/Ni/AC-CP electrode achieves 180 mF/cm^2 as shown in Figure 4d. The galvanostatic charge–discharge curves of graphite/Ni/AC-CP electrode betw-een −1.5 to 0 V are well symmetrical as shown in Figure 4e, indicating superior reversible redox reactions and good supercapacitive characteristic. The graphite/Ni/AC-CP electrode shows C_{sp} of 220 mF/cm^2 at current density of 4 mA/cm^2. The above results confirm good capacitive characteristic of graphite/Ni/AC-CP electrode. Additional, the graphite/Ni/AC-CP electrodes show excellent cycle life as

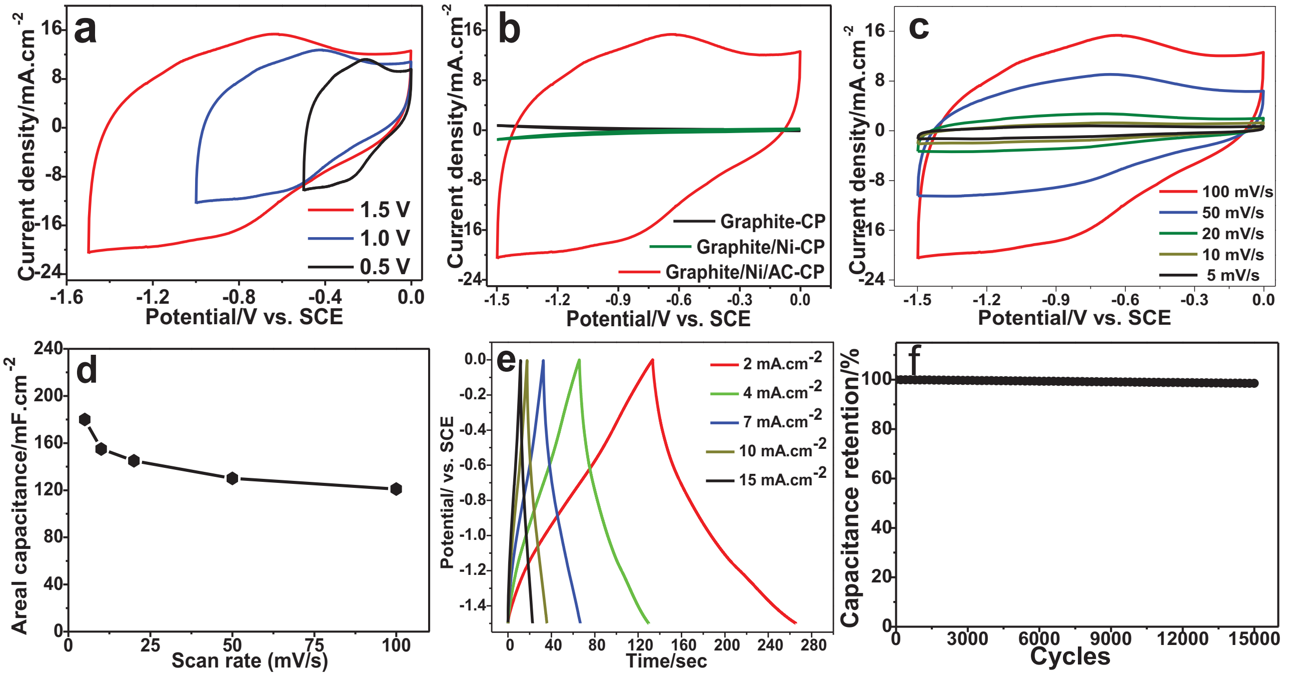

Figure 4. a) CVs of the graphite/Ni/AC-CP electrodes at different potential windows at 100 mV/s; b) CVs of graphite-CP, graphite/Ni-CP, and graphite/Ni/AC-CP electrodes at 100 mV/s; c) CVs of graphite/Ni/AC-CP electrode at various scan rates of 5–100 mV/s; d) Areal capacitance and capacitance retention of graphite/Ni/AC-CP electrode calculated from CV curves as a function of scan rate; e) Galvanostatic charge–discharge curves of graphite/Ni/AC-CP electrode at various current densities of 2–15 mA/cm^2; f) Cycling performance of graphite/Ni/AC-CP electrode for 15000 cycles.

shown in Figure 4f, which shows C_{sp} retention is ≈98% after 15 000 cycles.

The above-mentioned experimental results show that the fabricated graphite/Ni/Co_2NiO_4-CP and graphite/Ni/AC-CP have great potential as high-performance positive and negative electrodes, respectively. To test the feasibility of above electrodes, the solid-state ATFSCs were assembled using graphite/Ni/Co_2NiO_4-CP as positive electrodes and graphite/Ni/AC-CP as negative electrodes (named as graphite/Ni/Co_2NiO_4-CP//graphite/Ni/AC-CP ATFSCs) as shown in **Figure 5**a. The PVA/KOH gel was used as solid-gel electrolyte. The assembed graphite/Ni/Co_2NiO_4-CP//graphite/Ni/AC-CP ATFSC is shown in Figure 5c. The average thickness of the well-assembled ATFSC device is 0.5 mm and the average weight of electroactive material is 1.55 mg (based on Co_2NiO_4 and AC). The ATFSCs have excellent flexibility and well mechanical properties and can undergo severe blending as shown in Figure 5d,e, and they also own high electronic and ionic conductivity as shown in Nyquist plot in Figure S12. CVs of the graphite/Ni/Co_2NiO_4-CP//graphite/Ni/AC-CP ATFSCs measured in a two-electrode system at various potential windows are shown in Figure 5f. The maximum potential window of the ATFSCs can be chosen as large as 2.0 V. CVs of the ATFSC device all exhibit rectangular-like shapes at various scan rates as shown in Figure 5g, which reveals good capacitive behavior. The graphite/Ni/Co_2NiO_4-CP//graphite/Ni/AC-CP ATFSCs show a maximum volumetric C_{sp} (based on entire device including both the electrolyte and electrodes) of 7.6 F/cm^3 (247.6 F/g) at 5 mV/s. Figure 5h shows galvanostatic charge–discharge curves of the ATFSCs at different current densities, and the relative symmetry in these charge–discharge curves confirms the good capacitive behavior. The maximum volumetric C_{sp} of the ATFSCs at 4.0 mA/cm^2 is calculated 4.48 F/cm^3 (144.4 F/g), which is much higher than the values (0.3–1.5 F/cm^3) reported for most of the solid-state SCs at the same current density.[33–35]

More importantly, the electrochemical performance of the graphite/Ni/Co_2NiO_4-CP//graphite/Ni/AC-CP ATFSCs almost has no change under various distortion situations as shown in Figure 5i, confirming that the ATFSCs have very good remarkable mechanical flexibility. The long-term cycling stability of the ATFSCs was firstly evaluated by CV test at a high scan rate of 100 mV/s. As shown in Figure 5j, C_{sp} of the ATFSC shows very slow decrease during the first initial 5000 cycles at the normal state. Then, the device was continuously tested for 5000 cycles under 90° bending state and further 5000 cycles under 180° bending at the same scan rate. Finally, the ATFSCs recover to normal state to test the final 5000 cycles. After above 20000 cycles, the ATFSCs show 96.4% retention of the initial C_{sp}, indicating excellent cycling performance and flexibility. The similar high cycling stability of ATFSCs is also proved by galvanostatic charge–discharge test at 10 mA/cm^2 as shown in Figure 5j. The C_{sp} retention rate at such a high charge–discharge rate are comparable and even better than those reported for aqueous and solid-state asymmetrical SCs (ASCs), such as Co_9S_8//Co_3O_4@RuO_2 ASC (90.2% C_{sp} retention after 2000 cycles at 2.5 mA/cm^2),[36] RuO_2/graphene//graphene ASC (95% C_{sp} retention after 2000 cycles at 1.0 A/g),[37] and Ni_3S_2/

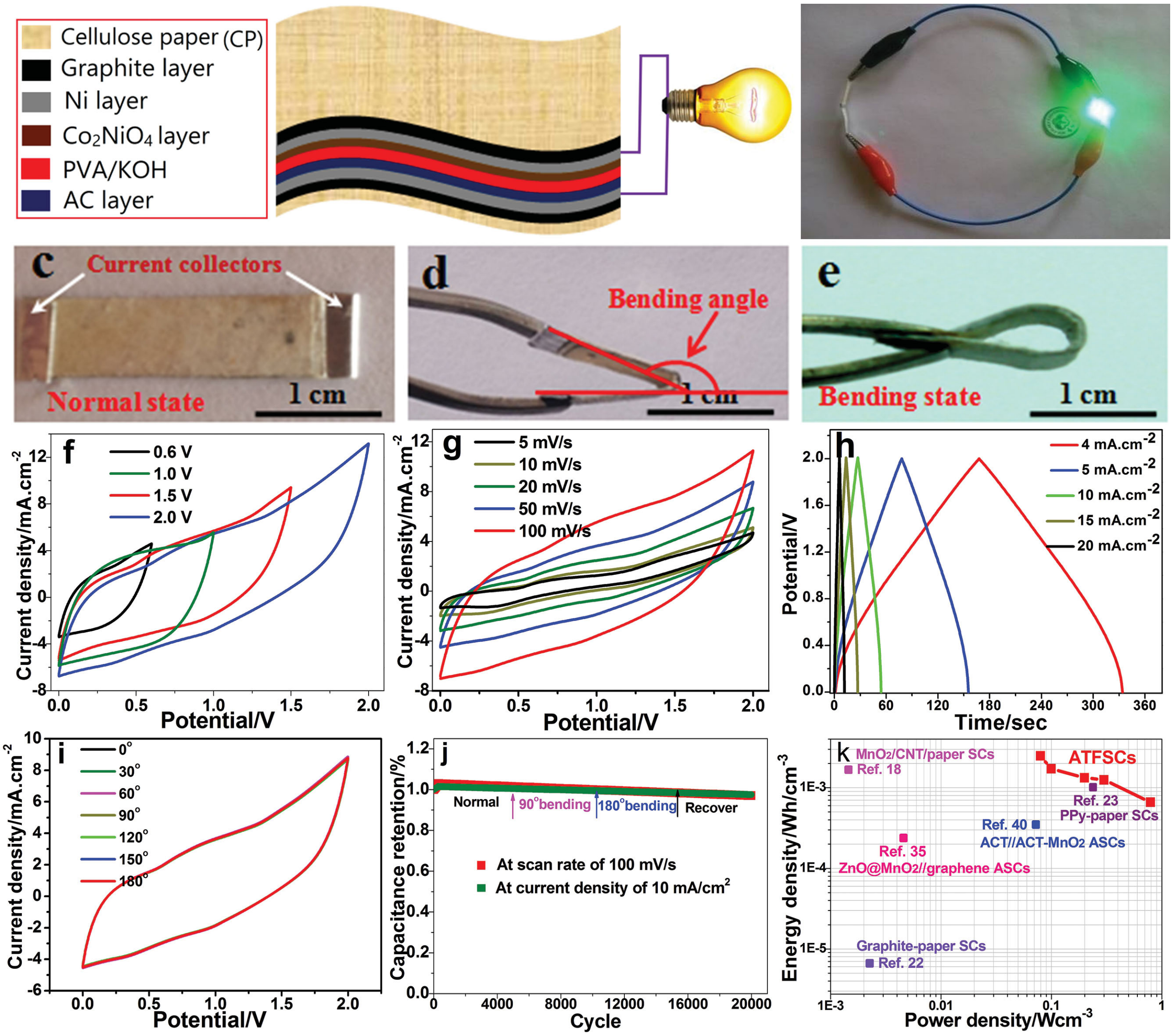

Figure 5. a) Schematic illustration for the assembled graphite/Ni/Co_2NiO_4-CP//graphite/Ni/AC-CP ATFSCs; (b) A light-emitting diode (LED) powered by 2 ATFSCs in series; The flexible assembled ATFSCs: c) normal state, d,e) bending states; f) CVs of the ATFSC device in different scan potential windows at 100 mV/s; g) CVs of the ATFSC device at different scan rates; h) Galvanostatic charge/discharge curves of ATFSC at different current densities; i) CVs of the ATFSC device under various bending states at 50 mV/s; j) Cycling performance of the ATFSC at different bending states for 20 000 cycles at 100 mV/s and 10 mA/cm^2; k) Ragone plots of the ATFSC devices. The maximum volumetric energy densities and power densities reported for other CP-based SCs and some ASC devices are added for comparison.[18,22,23,35,40]

MWCNT-NC//AC ASC (90% C_{sp} retention after 5000 cycles at 4.0 A/g).[38]

Figure 5k compares the volumetric energy and power densities of the graphite/Ni/Co_2NiO_4-CP//graphite/Ni/AC-CP ATFSCs to the values reported for the CP-based SCs and other ASCs. The maximum energy density of the as-fabricated ATFSCs is 2.48 mWh/cm^3 (80.0 Wh/kg) at 4.0 mA/cm^2 and the maximum power density is 0.79 W/cm^3 (25.6 kW/kg) at 20 mA/cm^2. More importantly, the obtained maximum volumetric energy density is considerably larger than those of recently reported CP-based SCs at the same current density, such as graphite/paper SCs (<0.1 mWh/cm^3),[21] PPy/paper SCs (<1.0 mWh/cm^3),[22] and MnO_2/CNT/paper SCs (<2.0 mWh/cm^3),[39] and some developed ASCs, such as ZnO@MnO_2//graphene ASCs (<0.23 mW·h/cm^3),[33] and activated carbon textile (ACT)//ACT-MnO_2 ASC (<0.35 mW h/cm^3).[40] Furthermore, the maximum volumetric power density of the as-fabricated ATFSCs also is much higher than those of above mentioned graphite/paper SCs,[21] PPy/paper SCs,[22] MnO_2/CNT/paper SCs,[39] ZnO@ MnO_2//graphene ASCs,[33] and ACT//ACT-MnO_2 ASC,[40] as shown in Figure 5k. Finally, to demonstrate the practical application of graphite/Ni/Co_2NiO_4-CP//graphite/Ni/AC-CP ATFSCs, two ATFSCs were connected in series to power green light-emitting diodes (LED, working voltage: 1.5 V) as shown in Figure 5b. Here we found that two devices could power a green light-emitting diode (LED) for ≈12 min after charging at 5 mA/cm^2 for 60 s, exhibiting high energy density and fast charge ability.

3. Conclusions

In summary, we have developed novel sandwich-structured graphite/Ni/Co_2NiO_4-CP as positive electrode and graphite/Ni/AC-CP as negative electrode for the flexible and high-performance ATFSCs. The graphite/Ni/Co_2NiO_4-CP electrodes were fabricated by a simple drawing-electrodeposition-anodic oxide combined method and they exhibit significantly enhanced electrochemical performance as compared to CP-based electrodes reported in literatures. The as-fabricated graphite/Ni/Co_2NiO_4-CP electrode shows a superior areal capacitance of 734 mF/cm^2 at 5 mV/s, which is almost the largest areal capacitance achieved by the CP-based electrodes. Furthermore, the graphite/Ni/Co_2NiO_4-CP electrode exhibits excellent cycling performance with ≈98% C_{sp} retention after 15 000 cycles. The significant improvement of the electrochemical performance of CP-based electrode is attributed to good conductivity, porous structure and Co_2NiO_4 nanosheets. In addition, the fabricated negative electrode of graphite/Ni/AC-CP also exhibits large areal capacitance and excellent cycling performance. The flexible and high-performance ATFSCs have been assembled with graphite/Ni/Co_2NiO_4-CP as positive electrode and graphite/Ni/AC-CP as negative electrode for electrochemical energy storage. This device can operate in a wide voltage window of 2.0 V and is able to deliver a maximum volumetric energy density of 2.48 mWh/cm^3 (80 Wh/kg) and volumetric power density of 0.79 W/cm^3 (25.6 kW/kg). Additionally, the device exhibits excellent cycling performance (<4% capacitance loss after 20 000 cycles). This work shows an important breakthrough in the design and fabrication of flexible and high-performance CP-based electrodes and ATFSCs.

Acknowledgements

This work was supported by NSFC (21073240 and 51173212), Natural Science Foundation of Guangdong Province (S2013020012833), Fundamental Research Fund for the Central Universities (13lgpy51), Fund of New Star Scientist of Pearl River Science and Technology of Guangzhou (2011J2200057), SRF for ROCS, SEM ([2012]1707), and New-Century Training Programme Foundation for the Talents by the State Education Commission (NCET-12–0560).

Received: June 9, 2014
Revised: July 26, 2014

---

[1] D. Tobjörk, R. Österbacka, *Adv. Mater.* **2011**, *23*, 1935–1961.
[2] A. Russo, B. Y. Ahn, J. J. Adams, E. B. Duoss, J. T. Bernhard, J. A. Lewis, *Adv. Mater.* **2011**, *23*, 3426–3430.
[3] C.-C. Hu, K.-H. Chang, M.-C. Lin, Y.-T. Wu, *Nano Lett.* **2006**, *6*, 2690–2695.
[4] H. Wang, L.-F. Cui, Y. Yang, H. S. Casalongue, J. T. Robinson, Y. Liang, Y. Cui, H. Dai, *J. Am. Chem. Soc.* **2010**, *132*, 13978–13980.
[5] L. Hu, H. Wu, F. L. Mantia, Y. Yang, Y. Cui, *ACS Nano* **2010**, *4*, 5843–5848.
[6] M. Kaempgen, C. K. Chan, J. Ma, Y. Cui, G. Gruner, *Nano Lett.* **2009**, *9*, 1872–1876.
[7] X. H. Xia, J. P. Tu, Y. Q. Zhang, X. L. Wang, C. D. Gu, X. B. Zhao, H. J. Fan, *ACS Nano* **2012**, *6*, 5531–5538.
[8] C. Guan, X. Li, Z. Wang, X. Cao, C. Soci, H. Zhang, H. J. Fan, *Adv. Mater.* **2012**, *24*, 4186–4190.
[9] S. Han, D. Wu, S. Li, F. Zhang, X. Feng, *Adv. Mater.* **2014**, *26*, 849–864.
[10] N. Liu, W. Ma, J. Tao, X. Zhang, J. Su, L. Li, C. Yang, Y. Gao, D. Golberg, Y. Bando, *Adv. Mater.* **2013**, *25*, 4925–4931.
[11] G. Zhang, X. W. Lou, *Adv. Mater.* **2013**, *25*, 976–979.
[12] X. Wang, B. Liu, Q. Wang, W. Song, X. Hou, D. Chen, Y. Cheng, G. Shen, *Adv. Mater.* **2013**, *25*, 1479–1486.
[13] J. Ren, L. Li, C. Chen, X. Chen, Z. Cai, L. Qiu, Y. Wang, X. Zhu, H. Peng, *Adv. Mater.* **2013**, *25*, 1155–1159.
[14] L.-F. Chen, Z.-H. Huang, H.-W. Liang, Q.-F. Guan, S.-H. Yu, *Adv. Mater.* **2013**, *25*, 4746–4752.
[15] Y. Meng, K. Wang, Y. Zhang, Z. Wei, *Adv. Mater.* **2013**, *25*, 6985–6990.
[16] L. Hu, J. W. Choa, Y. Yang, S. Jeong, F. L. Mantia, L.-F. Cui, Y. Cui, *Proc. Natl. Acad. Sci. U.S.A.* **2009**, *106*, 21490–21494.
[17] L. Hu, Y. Cui, *Energy Environ. Sci.* **2012**, *5*, 6423–6435.
[18] M. Kaempgen, C. K. Chan, J. Ma, Y. Cui, G. Gruner, *Nano Lett.* **2009**, *9*, 1872–1876.
[19] P.-C. Chen, G. Shen, Y. Shi, H. Chen, C. Zhou, *ACS Nano* **2010**, *4*, 4403–4411.
[20] Y. Cheng, H. Zhang, S. Lu, C. V. Varanasi, J. Liu, *Nanoscale* **2013**, *5*, 1067–1073.
[21] G. Zheng, L. Hu, H. Wu, X. Xie, Y. Cui, *Energy Environ. Sci.* **2011**, *4*, 3368–3373.
[22] L. Yuan, B. Yao, B. Hu, K. Huo, W. Chen, J. Zhou, *Energy Environ. Sci.* **2013**, *6*, 470–476.
[23] L. Yuan, X. Xiao, T. Ding, J. Zhong, X. Zhang, Y. Shen, B. Hu, Y. Huang, J. Zhou, Z. L. Wang, *Angew. Chem. Int. Ed.* **2012**, *51*, 4934–4938.
[24] K. Wandelt, *Surf. Sci. Rep.* **1982**, *2*, 1–121.
[25] a) Y. Roginskaya, O. Morozova, E. Lubnin, Y. Ulitina, G. Lopukhova, S. Trasatti, *Langmuir.* **1997**, *13*, 4621–4624; b) J. Li, S. Xiong, Y. Liu, Z. Ju, Y. Qian, *ACS Appl. Mater. Interfaces* **2013**, *5*, 981–988; c) Y. Lei, J. Li, Y. Wang, L. Gu, Y. Chang, H. Yuan, D. Xiao, *ACS Appl. Mater. Interfaces* **2014**, *6*, 1773–1780; d) G. Li, W. Li, K. Xu, R. Zou, Z. Chen, J. Hu, *J. Mater. Chem. A* **2014**, *2*, 7738–7741; e) M. Prabu, K. Ketpang, S. Shanmugam, *Nanoscale* **2014**, *6*, 3173–3181.
[26] J. Marco, J. Gancedo, M. Gracia, J. Gautier, F. Berry, *J. Solid State Chem.* **2000**, *153*, 74–81.
[27] J. Xiao, S. Yang, *J. Mater. Chem.* **2012**, *22*, 12253–12262.
[28] P. V. Kamath, G. H. Annal Therese, J. Gopalakrishnan, *J. Solid State Chem.* **1997**, *128*, 38–41.
[29] M. M. Natile, A. Glisenti, *Chem. Mater.* **2002**, *14*, 4895–4903.
[30] T. Choudhury, S. Saied, J. Sullivan, A. Abbot, *J. Phys. D: Appl. Phys.* **1989**, *22*, 1185–1188.
[31] H. Gao, F. Xiao, C. B. Ching, H. Duan, *ACS Appl. Mater. Interfaces* **2012**, *4*, 7020–7026.
[32] L. Huang, D. Chen, Y. Ding, Z. L. Wang, Z. Zeng, M. Liu, *ACS Appl. Mater. Interfaces* **2013**, *5*, 11159–11162.
[33] Z. Wang, Z. Zhu, J. Qiu, S. Yang, *J. Mater. Chem. C* **2014**, *2*, DOI: 10.1039/c3tc31476f.
[34] P. Yang, X. Xiao, Y. Li, Y. Ding, P. Qiang, X. Tan, W. Mai, Z. Lin, W. Wu, T. Li, H. Jin, P. Liu, J. Zhou, C. P. Wong, Z. L. Wang, *ACS Nano* **2013**, *7*, 2617–2626.
[35] M. F. El-Kady, V. Strong, S. Dubin, R. B. Kaner, *Science* **2012**, *335*, 1326–1330.

[36] J. Xu, Q. Wang, X. Wang, Q. Xiang, B. Liang, D. Chen, G. Shen, *ACS Nano* **2013**, *7*, 5453–5462.
[37] B. G. Choi, S.-J. Chang, H.-W. Kang, C. P. Park, H. J. Kim, W. H. Hong, S. Lee, Y. S. Huh, *Nanoscale* **2012**, *4*, 4983–4988.
[38] C. Dai, P. Chien, J. Lin, S. Chou, W. Wu, P. Li, K. Wu, T. Lin, *ACS Appl. Mater. Interfaces* **2013**, *5*, 12168–12174.
[39] Y. J. Kang, B. Kim, H. Chung, W. Kim, *Synth. Met.* **2010**, *160*, 2510–2514.
[40] L. Bao, X. Li, *Adv. Mater.* **2012**, *24*, 3246–3252.